

# SCIENTIFIC REPORTS

OPEN

## Investigation of spin-orbit torque using current-induced magnetization curve

Tomohiro Koyama, Yicheng Guan & Daichi Chiba 

Manipulation of magnetization using current-induced torque is crucial for magnetic recording devices. Recently, the spin-orbit torque (SOT) that emerges in a ferromagnetic thin film on a heavy metal is focused as a new scheme for magnetization switching in perpendicularly magnetized systems. Since the SOT provides a perpendicular effective field to the system, the formation of a magnetic multiple domain state because of Joule heating is suppressed in the magnetization reversal process. This means that high reliable switching is possible using the SOT. Here, by utilizing the SOT induced domain stability, we show that an electrical current directly injected to a perpendicularly magnetized Pt/Co/Pd system can magnetize itself, that is, current-induced magnetization process from multi to single domain state. A quantitative determination of the SOT is performed using the current-induced magnetization curve. The present results are of great importance as another approach to evaluate the SOT effect, as well as a demonstration of domain state switching caused by the SOT.

In magnetic recording devices, the information of a bit is retained as a magnetization direction. Spin-torque-induced magnetization switching<sup>1–6</sup> in magnetic tunnel junctions (MTJs) and current-induced domain wall (DW) displacement<sup>7–13</sup> in magnetic wires have been widely investigated as information writing methods in magnetic memory. Recently, a current-induced spin-orbit torque (SOT) emerging in a thin ferromagnetic film deposited on a heavy metal layer has been recognized as a new scheme for magnetization switching in perpendicularly magnetized materials<sup>14–19</sup>. Moreover, it is well known that current-induced DW dynamics is strongly affected by the SOT<sup>20–24</sup>.

The SOT is known to act on magnetizations as an effective field. This contributes to the magnetization switching and DW motion. More importantly, the SOT effective field also plays a role in stabilizing the domain state against current-induced Joule heating<sup>25,26</sup>, which is often a severe problem in devices based on current-induced torque<sup>27–29</sup>. Owing to this characteristic of the SOT, random multiple domain formation is suppressed even under high current density as much as  $10^{11}$ – $10^{12}$  A/m<sup>2</sup> during the magnetization reversal. In this letter, we show that in a perpendicularly magnetized Pt/Co/Pd structure with a multi domain (MD) state in thermal equilibrium (having no net magnetization), the magnetization of the system increases with injected current, and finally, a single domain (SD) state is created (see Fig. 1a). This “current-induced” magnetization process is observed only when an external in-plane magnetic field parallel to the current exists, indicating that the SOT is responsible for the effect. A quantitative determination of the SOT effective field from the current-induced magnetization curve is performed.

Figure 1b shows an optical microscope image of our device. The Hall bar component consists of asymmetrical Pt/Co/Pd layers deposited on a SiO<sub>2</sub>/intrinsic Si substrate (see also Methods). The width of the channel is 5 μm. Owing to the interface magnetic anisotropy at the Pt/Co and Co/Pd interfaces, the system exhibits perpendicular magnetic anisotropy PMA. The high PMA realizes an MD state with perpendicular magnetization near the Curie temperature (~370 K in our device). Four Cr/Cu electrodes are formed to apply the current and to detect the Hall resistance  $R_{\text{Hall}}$ . The definitions of each external magnetic field ( $\mu_0 H_x$ ,  $\mu_0 H_y$ , and  $\mu_0 H_z$ ) and the current flow along the  $x$ -axis are indicated in Fig. 1b. The temperature of the stage  $T_s$ , which is in thermal contact with the fabricated device, is controlled using a heater (see Methods).

Figure 2a shows the results of the  $R_{\text{Hall}}$  measurement when a dc current density  $J_{\text{dc}}$  of  $+2.8 \times 10^9$  A/m<sup>2</sup> is injected at room temperature ( $T_s = 304$  K).  $\mu_0 H_z$  is swept to obtain the curves.  $J_{\text{dc}}$  is determined by simply dividing

Department of Applied Physics, The University of Tokyo, Bunkyo, Tokyo, 113-8656, Japan. Correspondence and requests for materials should be addressed to T.K. (email: [tkoyama@ap.t.u-tokyo.ac.jp](mailto:tkoyama@ap.t.u-tokyo.ac.jp)) or D.C. (email: [dchiba@ap.t.u-tokyo.ac.jp](mailto:dchiba@ap.t.u-tokyo.ac.jp))

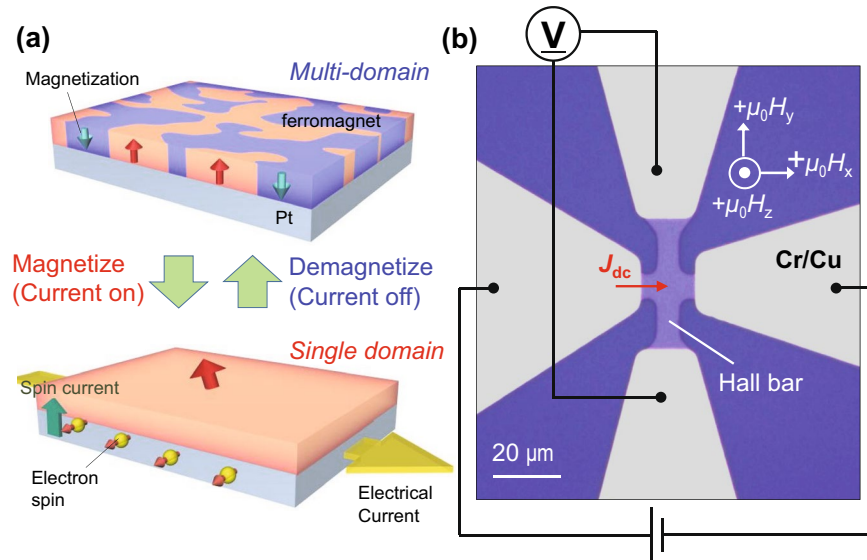


**Figure 1.** Current-induced magnetization process and schematic of device structure. **(a)** When electrical current is injected into thin ferromagnet/Pt layered structure, the system is gradually magnetized and finally, single magnetic domain structure appears. **(b)** Device image taken by an optical microscope. A Pt/Co/Pd Hall bar structure with  $5\ \mu\text{m}$  width is prepared. Grey regions indicate Cr/Cu electrodes. Current source and voltage meter are connected as shown in the figure. Directions of external magnetic fields ( $\mu_0H_x$ ,  $\mu_0H_y$  and  $\mu_0H_z$ ) are indicated by white arrows. The sign of electrical current is defined as positive when the current flows from left to right.

the current by the cross-sectional area of the metallic layers.  $R_{\text{Hall}}$  is proportional to the perpendicular component of the magnetization because of the anomalous Hall effect. A clear hysteresis loop with a coercivity  $\mu_0H_c$  of 2.4 mT is observed. The remanent value of  $R_{\text{Hall}}$  ( $R_{\text{Hall}}^{\text{r}}$ ) is almost equal to the saturation value, indicating that the SD state is stable at fields near zero.

Next,  $R_{\text{Hall}}$  measurements with  $J_{\text{dc}}$  sweeping are performed under constant in-plane magnetic fields. The procedure is as follows. First, the magnetization direction of the entire device is set upward by applying a  $\mu_0H_z$  of +30 mT. After returning to  $\sim 0$  T, a constant in-plane magnetic field ( $\mu_0H_x$  or  $\mu_0H_y$ ) of +38 mT is applied. Then,  $R_{\text{Hall}}$  is monitored with a sweeping  $J_{\text{dc}}$ . The positive (negative) sweep corresponds to a  $J_{\text{dc}}$  change from 0 to  $+1.7$  ( $-1.7$ )  $\times 10^{11}$  A/m<sup>2</sup>. Figure 2b and c show  $R_{\text{Hall}}$  as a function of  $J_{\text{dc}}$  measured under the application of  $\mu_0H_y$  and  $\mu_0H_x$ , respectively. As shown in the positive sweep (PS) in Fig. 2b,  $R_{\text{Hall}}$  abruptly decreases when a  $J_{\text{dc}}$  of  $+0.8 \times 10^{11}$  A/m<sup>2</sup> is applied, and drops toward zero in the region of  $J_{\text{dc}} > +0.8 \times 10^{11}$  A/m<sup>2</sup>, indicating that the MD state is formed at  $J_{\text{dc}} \geq 0.8 \times 10^{11}$  A/m<sup>2</sup> due to the Joule heating. A rapid decrease in  $R_{\text{Hall}}$  also appears symmetrically in the negative sweep (NS) case (see NS curve in Fig. 2b), suggesting that the Joule heating effect is independent of the  $J_{\text{dc}}$  direction.

By contrast, the situation is completely different when  $\mu_0H_x$ , which is parallel to  $J_{\text{dc}}$ , is applied. For the PS curve in Fig. 2c, a full  $R_{\text{Hall}}$  switching from positive to negative, which corresponds to the abrupt reversal of the magnetization direction from up to down, is observed at  $J_{\text{dc}} = +0.5 \times 10^{11}$  A/m<sup>2</sup>. In the NS curve, no switching occurs up to  $J_{\text{dc}} = -1.7 \times 10^{11}$  A/m<sup>2</sup>. When the sign of  $\mu_0H_x$  is reversed, switching is observed only for a negative  $J_{\text{dc}}$  (not shown). The switching direction in the present configuration is consistent with the SOT induced switching previously reported in the Pt/Co structure<sup>2,26</sup>. Although the sign of the spin Hall angle of the top Pd is the same as that of the Pt, the SOT in the present device is dominated by the spin current injection from the bottom Pt because the magnitude of the spin Hall angle of Pd is one order smaller than that of Pt<sup>30,31</sup>. We also checked that in a similar device structure, the top Pd effect on the SOT is negligibly small<sup>32</sup>. In order to evaluate the magnitude of SOT effective fields, *i.e.* the Slonczewski-like torque  $\mu_0H_{\text{SL}}$  and field-like torque  $\mu_0H_{\text{FL}}$ , the harmonic Hall measurement, which is widely used for the quantitative determination of the SOT<sup>33</sup>, was conducted for a similar device structure. The procedure is shown in the Supplementary Information.  $\mu_0H_{\text{SL}}$  and  $\mu_0H_{\text{FL}}$  are determined to be  $6.55 \pm 0.20$  mT/ $10^{11}$  A/m<sup>2</sup> and  $1.57 \pm 0.13$  mT/ $10^{11}$  A/m<sup>2</sup>, respectively. These values are close to those previously reported for Pt/ferromagnet bilayer structure<sup>22</sup>. Another important point here is that under  $\mu_0H_x$  application,  $|R_{\text{Hall}}|$  always represents a value close to saturation even at  $|J_{\text{dc}}| \geq 0.8 \times 10^{11}$  A/m<sup>2</sup>, indicating that the MD formation is completely suppressed against Joule heating. In the present case, the magnetization experiences a finite perpendicular effective field  $\mu_0H_{\text{eff}}$  derived from  $\mu_0H_{\text{SL}}$  because the magnetization tilts slightly toward the  $x$ -direction. When the current direction is the same as the  $\mu_0H_x$  direction, the sign of  $\mu_0H_{\text{eff}}$  becomes negative in the Pt/Co system. As a result, the SD state becomes stable because of the gain by the Zeeman energy reduction. Thus, the SOT plays an important role in stabilizing the SD state.

In the above experiments,  $T_d$  was increased by injecting a current. In the following, the MD state at thermal equilibrium is prepared by simply increasing  $T_d$  using a heater. Figure 3a shows the results of the Hall measurements performed at  $T_s = 343$  K.  $J_{\text{dc}}$  for this measurement is  $2.8 \times 10^9$  A/m<sup>2</sup>, and the Joule heating effect is negligibly

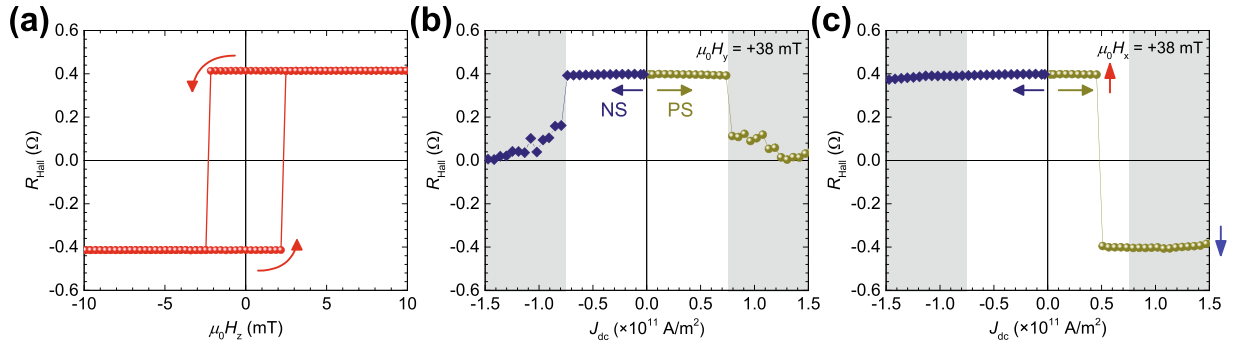


**Figure 2.** Anomalous Hall measurement under various dc currents. (a) Results of anomalous Hall resistance  $R_{\text{Hall}}$  measurement by sweeping perpendicular field  $\mu_0 H_z$ . Densities of dc current  $J_{\text{dc}}$  used here are  $+2.8 \times 10^9 \text{ A/m}^2$ . Sweep rate of  $\mu_0 H_z$  was  $\sim 0.04 \text{ mT/s}$ . Measurements were performed at stage temperature of 304 K. Red arrows indicate the sweep direction. (b,c)  $R_{\text{Hall}}$  as a function of  $J_{\text{dc}}$  obtained under  $\mu_0 H_y$  (b) and  $\mu_0 H_x$  (c) of  $+38 \text{ mT}$ . Shaded area indicates the  $J_{\text{dc}}$  region where multiple domain state appears under  $y$ -field. The error bar, which is the standard deviation of two data points, is smaller than the symbols.

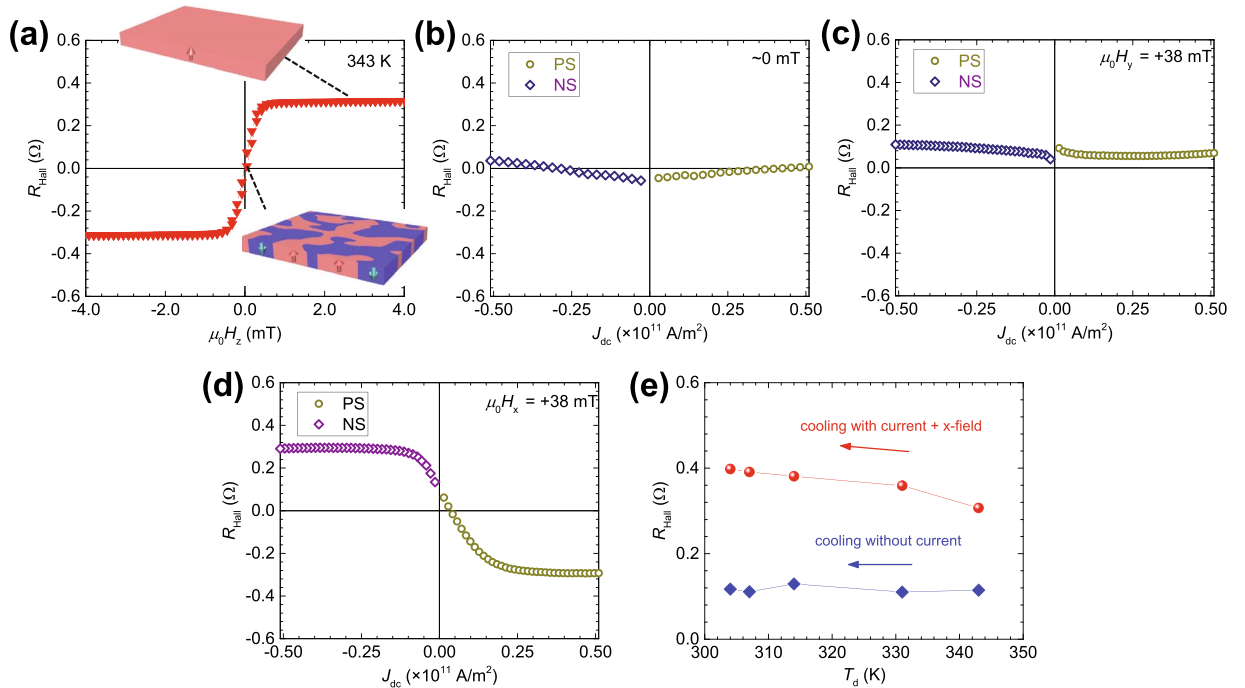


**Figure 3.** Current sweep measurement under 343 K. (a)  $\mu_0 H_z - R_{\text{Hall}}$  curve obtained at stage temperature  $T_d$  of 343 K.  $J_{\text{dc}}$  of  $+2.8 \times 10^9 \text{ A/m}^2$  is used for the measurement. (b–d)  $J_{\text{dc}}$  dependences of  $R_{\text{Hall}}$  measured under (b) 0 T, (c)  $\mu_0 H_y$ , and (d)  $\mu_0 H_x$  of  $+38 \text{ mT}$ , respectively. Yellow (purple) points indicate results for the positive (negative) current sweep. (e) Results of  $T_d$  cooling experiment.  $T_d$  is reduced from 343 K to 304 K with injecting  $J_{\text{dc}}$  of  $-0.25 \times 10^{11}$  (red) and  $-2.8 \times 10^9 \text{ A/m}^2$  (blue) under  $\mu_0 H_x = +38 \text{ mT}$ . The error bar, which is the standard deviation of two data points, is smaller than the symbols.

small. In this case, an anhyseric  $R_{\text{Hall}}$  curve with the almost zero remanent is observed. This indicates that the MD state is realized and the system is demagnetized. Figure 3b shows  $R_{\text{Hall}}$  as a function of  $J_{\text{dc}}$  obtained under  $\mu_0 H_z$  of  $\sim 0 \text{ T}$ .  $R_{\text{Hall}}$  is almost independent of  $J_{\text{dc}}$  in the range of  $\pm 0.5 \times 10^{11} \text{ A/m}^2$ . Similarly, no change in  $R_{\text{Hall}}$  is observed for a  $\mu_0 H_y$  of  $+38 \text{ mT}$ , as shown in Fig. 3c. The slight  $R_{\text{Hall}}$  deviation from zero is probably due to the small  $z$ -component of the field. The slight  $J_{\text{dc}}$  dependence on  $R_{\text{Hall}}$  shown in Fig. 3b and c might be a result of the Oersted field. Based on these results, it can be concluded that in both cases, the MD state is kept under current injection. The result obtained under  $\mu_0 H_x = +38 \text{ mT}$  is completely different, as shown in Fig. 3d. For a small  $J_{\text{dc}}$ ,  $R_{\text{Hall}}$  showed an intermediate value, indicating that the MD state remains. However, a clear increase and decrease in  $R_{\text{Hall}}$  with increasing current toward the negative and positive magnetization directions, respectively, are observed. For both current directions,  $R_{\text{Hall}}$  saturates above  $|J_{\text{dc}}| = 0.1\text{--}0.2 \times 10^{11} \text{ A/m}^2$  and the  $R_{\text{Hall}}$  saturation values are consistent with those for the SD state. This result indicates that magnetization process of the system is caused by the SOT.

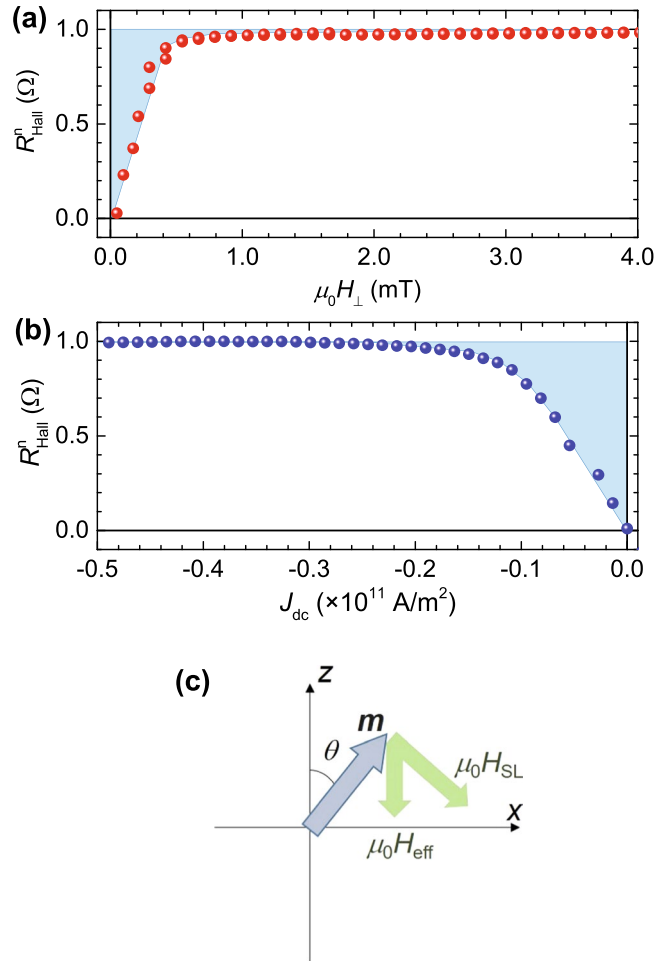


**Figure 4.** Quantitative determination of SOT effective field. **(a)** Normalized  $R_{\text{Hall}}$  as a function of  $\mu_0 H_z$  in range from 0 to +4.0 mT at 343 K. **(b)** Negative  $J_{\text{dc}}$  dependence of normalized  $R_{\text{Hall}}$  under  $\mu_0 H_x$  of +38 mT at 343 K. Zeeman energy gains by  $\mu_0 H_z$  and perpendicular component of the SOT effective field  $\mu_0 H_{\text{eff}}$  correspond to areas of coloured region indicated in a and b, respectively. The error bar, which is the standard deviation of two data points, is smaller than the symbols. **(c)** Schematic illustration displaying directions of the longitudinal effective field due to the Slonczewski-like torque  $\mu_0 H_{\text{SL}}$  and  $\mu_0 H_{\text{eff}}$  with respect to the magnetization direction  $m$ . Electrical current flows in +x direction.

In order to check whether the device is fully in the SD state, a cooling experiment under current is carried out. The procedure is as follows. After making  $R_{\text{Hall}}$  saturation using current under  $\mu_0 H_x = +38$  mT,  $T_d$  is gradually decreased from 343 K to room temperature with remaining the current and x-field application.  $J_{\text{dc}}$  of  $-0.25 \times 10^{11}$  A/m<sup>2</sup> is continuously applied during the cooling. During the  $T_d$  decrease,  $R_{\text{Hall}}$  is monitored. The result is shown in Fig. 3e. One can see that  $R_{\text{Hall}}$  gradually increases with decreasing  $T_d$  and at room temperature it shows  $\sim 0.4 \Omega$ , which is the value for the SD state. This indicates that the SD state is created by the current at 343 K and is maintained during cooling. On the other hand, when the above experiment is performed with an injection of  $J_{\text{dc}} = -2.8 \times 10^9$  A/m<sup>2</sup>,  $R_{\text{Hall}}$  shows a small value of  $\sim 0.1 \Omega$  even at room temperature, suggesting that the MD state formed at 343 K is retained even at room temperature. Therefore, the  $R_{\text{Hall}}$  saturation in Fig. 3(d) corresponds to the complete SD state, *i.e.* a situation where no domain with an opposite magnetization exists in the device is realized against thermal agitation. The result presented here demonstrates that the magnetization curve of Pt/Co/Pd system can be obtained by only sweeping electrical current owing to the stability caused by the SOT. In addition, the magnetization direction can be reversibly controlled by simply changing the current polarity.

The magnetization processes shown in Fig. 3(a) and (d) are caused by  $\mu_0 H_z$  and  $\mu_0 H_{\text{eff}}$ , which is proportional to  $J_{\text{dc}}$ , respectively. The current-induced magnetization process is expected to develop with the DW motion in the current direction, while the magnetic domains isotropically expands when the magnetization process is caused by the external field. Here, we focus on the gains of the Zeeman energy for each case and determine  $\mu_0 H_{\text{eff}}$ , and consequently  $\mu_0 H_{\text{SL}}$ , by comparing them. First,  $E_z$  obtained by  $\mu_0 H_z$  ( $E_{z-H}$ ) is calculated for the up magnetization case. Figure 4(a) shows the normalized  $R_{\text{Hall}}$  ( $R_{\text{Hall}}^n$ ) as a function of  $\mu_0 H_z$  in the range from 0 to +4.0 mT.  $E_{z-H}$  can be calculated using the following equation:

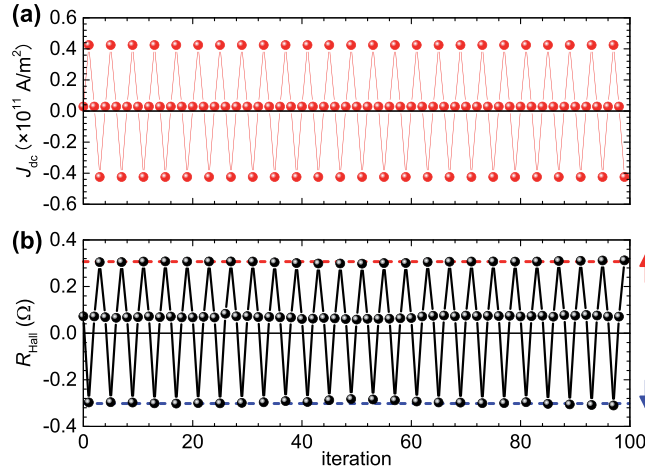


**Figure 5.** Alternative domain state switching. (a) Sequence of pulsed  $J_{dc}$  injection.  $J_{dc}$ s of  $+0.4 \times 10^{11}$ ,  $+2.8 \times 10^9$ , and  $-0.4 \times 10^{11}$  A/m<sup>2</sup> are repeatedly injected into the device. The pulse duration of each  $J_{dc}$  is 1.0 s. (b) Monitored  $R_{Hall}$  during alternative  $J_{dc}$  injection. Dashed lines indicate the saturation values of  $R_{Hall}$  in single domain state.

$$E_{Z-H} = M_s \int_0^1 dR_{Hall}^n \mu_0 H_z, \quad (1)$$

where  $M_s$  is the saturation magnetization of the system. The integral term of (1) is defined by the coloured area of Fig. 4(a), and  $E_{Z-H}/M_s$  is determined to be 0.180 mT. Subsequently, using the current-induced magnetization curve shown in Fig. 3(d),  $E_z$  resulting from  $\mu_0 H_{eff}$  ( $E_{Z-}$ ) is calculated.  $R_{Hall}^n$  as a function of  $J_{dc}$  in the negative  $J_{dc}$  sweep, where the positive  $\mu_0 H_{eff}$  is applied to the system, is shown in Fig. 4(b). The small  $J_{dc}$  offset is corrected in this figure. Since  $\mu_0 H_{eff}$  is expected to be proportional to  $J_{dc}$ ,  $E_{Z-}$  can be determined from the following:

$$E_{Z-} = -M_s \int_0^1 dR_{Hall}^n \alpha J_{dc}, \quad (2)$$

where  $\alpha$  is the constant value defined as  $\mu_0 H_{eff}/J_{dc}$ . The calculation of  $E_{Z-}/M_s$  is done in the same manner and is determined to be  $0.662\alpha \times 10^{10}$  A/m<sup>2</sup>. The same calculations are performed for the down magnetization case. Assuming  $E_{Z-H}/M_s = E_{Z-}/M_s$ ,  $\alpha = 2.51 \pm 0.01$  mT/ $10^{11}$  A/m<sup>2</sup> is finally obtained.

Next, we calculated  $\mu_0 H_{SL}$  (per  $10^{11}$  A/m<sup>2</sup>) using  $\mu_0 H_{eff}$  determined above. Figure 4(c) shows a schematic where the direction of  $\mu_0 H_{SL}$  under the  $x$ -field is denoted.  $\mu_0 H_{eff}$  is the perpendicular component of  $\mu_0 H_{SL}$  and  $\theta$  is the tilting angle of the magnetization from the  $z$ -axis. Thus,  $\mu_0 H_{SL}$  is expressed as  $\mu_0 H_{eff}/\sin\theta$ . From the  $x$ -field dependence of the anomalous Hall resistance,  $\theta$  at  $\mu_0 H_x = +38$  mT is approximately  $19^\circ$  in our Pt/Co/Pd structure. Therefore,  $\mu_0 H_{SL}$  of  $7.67 \pm 0.04$  mT/ $10^{11}$  A/m<sup>2</sup> is obtained. This value shows good agreement with that obtained by the harmonic measurement in our Pt/Co/Pd system.  $\mu_0 H_{eff}$  was also calculated using a Langevin fit and the result is consistent with the direct Zeeman energy calculation (see Supplementary Information). The calculation results presented here indicate that the SOT effective field can be quantitatively determined from the current-induced magnetization curve.

Finally, we demonstrate current-induced alternate switching between the MD and SD states. Figure 5(a) shows the sequence of  $J_{dc}$  injection into the device. A pulsed  $J_{dc}$  with three values of  $+0.4 \times 10^{11}$ ,  $+2.7 \times 10^9$ , and  $-0.4 \times 10^{11}$  A/m<sup>2</sup> is injected in series to create the SD state with up and down magnetization. The duration of each  $J_{dc}$  pulse is 1.0 s, and a  $\mu_0 H_x$  of +38 mT is applied during the measurement. The  $R_{Hall}$  value is measured during the pulse injection, and the result is shown in Fig. 5(b). Maximum and minimum  $R_{Hall}$  values corresponding to the up and down SD states appear alternately with the injections of  $+0.4$  and  $-0.4 \times 10^{11}$  A/m<sup>2</sup>. At  $J_{dc} = 2.7 \times 10^9$  A/m<sup>2</sup>,  $R_{Hall}$  always exhibits an intermediate value, that is, the MD state is restored. We checked that the current-induced SD state returns to the MD state within 1 ms after pulse off. This result indicates that an arbitrary switching of domain states between MD and SD can be achieved by injecting a current. Although in the present case, 1-ns-long pulses were used for the convenience of the measurement, sub-ns domain state switching is expected to be possible because the SOT induced magnetization switching occurs in this time scale<sup>34</sup>.

When the SOT effectively acts on the magnetization, the electrical current flowing in the system enhances the stability of the single domain state. In this study, owing to this domain stability, we show that the magnetization curve of the nonmagnetic/ferromagnetic metal structure can be obtained by sweeping electrical current, while it is conventionally obtained by sweeping external magnetic field. This effect would be marked in smaller size applicable to current IT devices because the SOT field is proportional to the current density flowing in the heavy metal layer. Anisotropy-wedged film<sup>16</sup>, an interlayer exchange coupled system<sup>17</sup>, and an antiferromagnet/ferromagnet layered structure<sup>18</sup>, where in-plane field free magnetization switching by the SOT was achieved, may also enable

domain state switching without an in-plane field. In addition, this work offers a novel method to determine the SOT effective field from the current-induced magnetization curve.

## Methods

**Film deposition and device fabrication.** Multilayered Ta (2.7 nm)/Pt (3.0)/Co(0.36)/Pd (0.8) film was deposited on a thermally oxidized Si substrate using rf sputtering, and a 0.5-nm-thick Ta layer was formed on the film as a cap. The base pressure of the sputter chamber was below  $1.0 \times 10^{-6}$  Pa, and Xe process gas was used for the deposition. The X-ray diffraction profile indicates that the Pt layer has an fcc (111) texture. The film was patterned into a Hall bar structure by photolithography and Ar ion milling. Cr (1.0)/Cu (100) electrodes were deposited by thermal evaporation and defined by a lift-off process using photolithography.

**Measurement setup.** Measurements were performed using a probe system in which a vector magnetic field can be applied. The device temperature was controlled by a plate-shaped heater placed under the device and monitored using a Pt thermometer (Pt-100). A current source (Yokogawa 7651) and nano-voltmeter (Keithley 2182A) were used for anomalous Hall measurements.

## References

1. Brataas, A., Kent, A. D. & Ohno, H. Current-induced torques in magnetic materials. *Nature Mater.* **11**, 372–381 (2012).
2. Berger, L. Emission of spin waves by a magnetic multilayer traversed by a current. *Phys. Rev. B* **54**, 9353–9358 (1996).
3. Slonczewski, J. C. Current-driven excitation of magnetic multilayers. *J. Magn. Magn. Mater.* **159**, L1–L7 (1996).
4. Huai, Y., Albert, F., Nguyen, P., Pakala, M. & Valet, T. Observation of spin-transfer switching in deep submicron-sized and low-resistance magnetic tunnel junctions. *Appl. Phys. Lett.* **84**, 3118 (2004).
5. Ikeda, S. *et al.* A perpendicular-anisotropy CoFeB-MgO magnetic tunnel junction. *Nature Mater.* **9**, 721–724 (2010).
6. Amiri, P. K. *et al.* Switching current reduction using perpendicular anisotropy in CoFeB-MgO magnetic tunnel junctions. *Appl. Phys. Lett.* **98**, 112507 (2011).
7. Yamaguchi, A. *et al.* Real-space observation of current-driven domain wall motion in submicron magnetic wires. *Phys. Rev. Lett.* **92**, 077205 (2004).
8. Vernier, N., Allwood, D. A., Atkinson, D., Cooke, M. D. & Cowburn, R. P. Domain wall propagation in magnetic nanowires by spin-polarized current injection. *Europhys. Lett.* **65**, 526–532 (2004).
9. Yamanouchi, M., Chiba, D., Matsukura, F. & Ohno, H. Current-induced domain-wall switching in a ferromagnetic semiconductor structure. *Nature* **428**, 539–542 (2004).
10. Togawa, Y. *et al.* Domain Nucleation and Annihilation in Uniformly Magnetized State under Current Pulses in Narrow Ferromagnetic Wires. *Jpn. J. Appl. Phys.* **45**, L1322–L1324 (2006).
11. Parkin, S. S. P., Hayashi, M. & Thoms, L. Magnetic Domain-Wall Racetrack Memory. *Science* **320**, 190–194 (2008).
12. Hayashi, M., Thoms, L., Moriya, R., Rettner, C. & Parkin, S. S. P. Current-Controlled Magnetic Domain-Wall Nanowire Shift Register. *Science* **320**, 209–211 (2008).
13. Koyama, T. *et al.* Observation of the intrinsic pinning of a magnetic domain wall in a ferromagnetic nanowire. *Nature Mater.* **10**, 194–197 (2011).
14. Miron, I. M. *et al.* Perpendicular switching of a single ferromagnetic layer induced by in-plane current injection. *Nature* **476**, 189–193 (2011).
15. Liu, L. *et al.* Spin-torque switching with the giant spin Hall effect of tantalum. *Science* **336**, 555–558 (2012).
16. Yu, G. *et al.* Switching of perpendicular magnetization by spin-orbit torques in the absence of external magnetic fields. *Nature Nanotechnol.* **9**, 548–554 (2014).
17. Lau, Y.-C., Betto, D., Rode, K., Coey, J. M. D. & Stamenov, P. Spin orbit torque switching without an external field using interlayer exchange coupling. *Nature Nanotechnol.* **11**, 758–762 (2014).
18. Fukami, S., Zhang, C., DuttaGupta, S., Kurenkov, A. & Ohno, H. Magnetization switching by spin-orbit torque in an antiferromagnet-ferromagnet bilayer system. *Nature Mater.* **15**, 535–541 (2016).
19. Van den Brink, A. *et al.* Field-free magnetization reversal by spin-Hall effect and exchange bias. *Nature Commun.* **7**, 10854 (2016).
20. Miron, I. M. *et al.* Fast current-induced domain wall motion controlled by the Rashba effect. *Nature Mater.* **10**, 419–423 (2011).
21. Haazen, P. P. J. *et al.* Domain wall depinning governed by the spin Hall effect. *Nature Mater.* **12**, 299–303 (2013).
22. Emori, S., Bauer, U., Ahn, S.-M., Martinez, E. & Beach, G. S. D. Current-driven dynamics of chiral ferromagnetic domain walls. *Nature Mater.* **12**, 611–616 (2013).
23. Ryu, K.-S., Thoms, L., Yang, S.-H. & Parkin, S. Chiral spin torque at magnetic domain walls. *Nature Nanotechnol.* **8**, 527–533 (2013).
24. Yang, S.-H., Ryu, K.-S. & Parkin, S. Domain-wall velocities of up to  $750 \text{ ms}^{-1}$  driven by exchange-coupling torque in synthetic antiferromagnets. *Nature Nanotechnol.* **10**, 221–226 (2015).
25. Miron, I. M. *et al.* Current-driven spin torque induced by the Rashba effect in a ferromagnetic metal layer. *Nature Materials* **9**, 230–234 (2010).
26. Liu, L., Lee, O. J., Gudmundsen, T. J., Ralph, D. C. & Buhrman, R. A. Current-Induced Switching of Perpendicularly Magnetized Magnetic Layers Using Spin Torque from the Spin Hall Effect. *Phys. Rev. Lett.* **109**, 096602 (2012).
27. Fuchs, G. D. *et al.* Adjustable spin torque in magnetic tunnel junctions with two fixed layers. *Appl. Phys. Lett.* **86**, 152509 (2005).
28. Yamaguchi, A. *et al.* Effect of Joule heating in current-driven domain wall motion. *Appl. Phys. Lett.* **86**, 012511 (2005).
29. Cormier, M. *et al.* Effect of electrical current pulses on domain walls in Pt/Co/Pt nanotracks with out-of-plane anisotropy: Spin transfer torque and Joule heating. *Phys. Rev. B* **81**, 024407 (2010).
30. Ando, K. & Saito, E. Inverse spin-Hall effect in palladium at room temperature. *J. Appl. Phys.* **108**, 113925 (2010).
31. Tang, Z. *et al.* Temperature Dependence of Spin Hall Angle of Palladium. *Appl. Phys. Exp.* **6**, 083001 (2013).
32. Koyama, T. & Chiba, D. Determination of effective field induced by spin-orbit torque using magnetic domain wall creep in Pt/Co structure. *Phys. Rev. B* **92**, 220402(R) (2015).
33. Kim, J. *et al.* Layer thickness dependence of the current-induced effective field vector in Ta/CoFeB/MgO. *Nature Materials* **12**, 240–245 (2013).
34. Garello, K. *et al.* Ultrafast magnetization switching by spin-orbit torques. *Appl. Phys. Lett.* **105**, 212402 (2014).

## Acknowledgements

The authors thank S. Ono, A. Tsukazaki, F. Matsukura, and H. Ohno for their technical help. This work was partly supported by the Grants-in-aid for Young Scientists (A) (No. 15H05419), Scientific Research (S) (No. 25220604), Specially promoted Research (No. 15H05702) from JSPS, the Murata Science Foundation, and Spintronics Research Network of Japan.

### Author Contributions

T.K. and D.C. planned the study. T.K. deposited the film and fabricated the device. T.K. and Y.G. performed the measurement and data analysis. T.K. wrote the manuscript with input from D.C. All authors discussed the results.

### Additional Information

**Supplementary information** accompanies this paper at doi:[10.1038/s41598-017-00962-7](https://doi.org/10.1038/s41598-017-00962-7)

**Competing Interests:** The authors declare that they have no competing interests.

**Publisher's note:** Springer Nature remains neutral with regard to jurisdictional claims in published maps and institutional affiliations.



**Open Access** This article is licensed under a Creative Commons Attribution 4.0 International License, which permits use, sharing, adaptation, distribution and reproduction in any medium or format, as long as you give appropriate credit to the original author(s) and the source, provide a link to the Creative Commons license, and indicate if changes were made. The images or other third party material in this article are included in the article's Creative Commons license, unless indicated otherwise in a credit line to the material. If material is not included in the article's Creative Commons license and your intended use is not permitted by statutory regulation or exceeds the permitted use, you will need to obtain permission directly from the copyright holder. To view a copy of this license, visit <http://creativecommons.org/licenses/by/4.0/>.

© The Author(s) 2017